

Quantum-Confined Tunable Ferromagnetism on the Surface of a van der Waals

Antiferromagnet NaCrTe₂

Yidian Li¹, Xian Du¹, Junjie Wang^{2,3}, Runzhe Xu¹, Wenxuan Zhao¹, Kaiyi Zhai¹, Jieyi Liu⁴, Houke Chen⁴,
Yiheng Yang⁴, Nicolas C. Plumb⁵, Sailong Ju⁵, Ming Shi⁵, Zhongkai Liu^{6,7}, Jiangang Guo², Xiaolong
Chen², Yulin Chen^{4,6,7*}, and Lexian Yang^{1,8,9*}

¹ *State Key Laboratory of Low Dimensional Quantum Physics, Department of Physics, Tsinghua University,
Beijing 100084, China.*

² *Lab for Advanced Materials and Electron Microscopy, Institute of Physics, Chinese Academy of Sciences,
Beijing 100083, China*

³ *University of Chinese Academy of Sciences, Beijing 100049, China.*

⁴ *Department of Physics, Clarendon Laboratory, University of Oxford, Parks Road, Oxford OX1 3PU, UK.*

⁵ *Photon Science Division, Paul Scherrer Institut, CH-5232, Villigen, PSI, Switzerland*

⁶ *School of Physical Science and Technology, ShanghaiTech University, Shanghai 201210, China.*

⁷ *ShanghaiTech Laboratory for Topological Physics, Shanghai 200031, China.*

⁸ *Frontier Science Center for Quantum Information, Beijing 100084, China.*

⁹ *Collaborative Innovation Center of Quantum Matter, Beijing 100084, China.*

e-mail: YLC: yulin.chen@physics.ox.ac.uk; LXY: lxyang@tsinghua.edu.cn

Abstract

The surface of three-dimensional materials provides an ideal and versatile platform to explore quantum-confined physics. Here, we systematically investigate the electronic structure of Na-intercalated CrTe_2 , a van der Waals antiferromagnet, using angle-resolved photoemission spectroscopy and *ab-initio* calculations. The measured band structure deviates from the calculation of bulk NaCrTe_2 but agrees with that of ferromagnetic monolayer CrTe_2 . Consistently, we observe an unexpected exchange splitting of the band dispersions, persisting well above the Néel temperature of bulk NaCrTe_2 . We argue that NaCrTe_2 features a quantum-confined 2D ferromagnetic state in the topmost surface layer due to strong ferromagnetic correlation in the CrTe_2 layer. Moreover, the exchange splitting and the critical temperature can be controlled by surface doping of alkali-metal atoms, suggesting a feasible tunability of the surface ferromagnetism. Our work not only presents a simple platform to explore tunable 2D ferromagnetism but also provides important insights into the quantum-confined low-dimensional magnetic states.

Two-dimensional (2D) magnetism violating the Mermin-Wagner theorem¹ not only features great scientific significance but also promises application potentials in electronic and spintronic devices²⁻⁶. Upon searching for robust 2D magnetic materials with desirable tunability, many interesting systems have emerged with attractive properties, such as the intrinsic long-range ferromagnetism in CrI₃ and Cr₂Ge₃Te₆^{7, 8}, room-temperature ferromagnetism in ultrathin films of different chalcogenides⁹⁻¹¹, and quantum anomalous Hall effect in 5-layer MnBi₂Te₄¹². Van der Waals (vdW) heterostructures were also fabricated to explore the interplay between magnetism, topology, superconductivity, and ferroelectrics^{2, 4, 5, 13}. However, the requirement for high-quality thin films or heterostructures makes it challenging to further investigate 2D magnetic systems. Alternatively, the surface of 3D materials naturally provides a versatile playground for exploring quantum-confined 2D physics, including 2D magnetism¹⁴⁻¹⁶.

Among various 2D magnetic platforms, transition metal chalcogenides with high magnetic transition temperatures and feasible tunability have invigorated tremendous research interests^{9, 17, 18}. A prototypical example is the room-temperature ferromagnetism in ultrathin 1T-CrTe₂ films^{11, 19, 20}. They exhibit many intriguing magnetic properties, including large magnetic anisotropy at room temperature¹¹, thickness-tunable Curie temperature²¹, and colossal anomalous Hall effect²². However, air-unstable CrTe₂ films can only be fabricated using molecular beam epitaxy or chemical vapor deposition, and the bulk CrTe₂ crystal is metastable, which limits further investigation of CrTe₂-based 2D magnetism. Some crucial properties of CrTe₂ films, such as the Curie temperature and ferromagnetic (FM) mechanism, remain elusive^{11, 19, 21, 23-25}.

On the other hand, the metastable CrTe_2 crystal can be stabilized by intercalating alkali-metal atoms, as exemplified by NaCrTe_2 , an A-type antiferromagnet with Néel temperature $T_N = 106 \text{ K}$ ^{26, 27}. It retains the in-plane ferromagnetism in each layer^{27, 28}, which provides an alternative route to explore the intriguing CrTe_2 -based 2D magnetism on the sample surface. In addition, NaCrTe_2 itself exhibits a spin-flip transition into FM spin alignment under a magnetic field accompanied by a giant negative magnetoresistance effect and tunable perpendicular magnetic anisotropy^{26, 27}, promising important applications in magneto-electronic devices.

In this work, we systematically investigate the electronic structure of vdW antiferromagnet NaCrTe_2 using high-resolution angle-resolved photoemission spectroscopy (ARPES) and *ab-initio* calculations. The surface layer of NaCrTe_2 is an interesting analog to the monolayer CrTe_2 or Na-decorated CrTe_2 . The measured band structure is different from the calculation of bulk NaCrTe_2 in the antiferromagnetic (AFM) state. On the contrary, the calculation of FM CrTe_2 monolayer well reproduces the experiments. Consistently, we observe an unexpected exchange splitting of energy bands that characterizes a quantum-confined surface FM state with a critical temperature well above T_N of bulk NaCrTe_2 . Moreover, the surface FM state can be effectively controlled by surface doping of alkali-metal atoms. The quantum-confined ferromagnetism on the AFM bulk NaCrTe_2 provides a simple platform to explore the rich physics and application potentials of 2D magnetism in CrTe_2 -based systems.

NaCrTe_2 crystallizes into a layered structure with the space group $P-3m1$ (No. 164), as

schematically shown in Figure 1a. The bondless Na atoms occupy the octahedral interstitial sites between CrTe₂ layers (Figure 1a) and expand the lattice constants of the CrTe₂ layers into the FM region in its magnetic phase diagram^{29, 30}. Figure 1b shows the hexagonal Brillouin zone and its surface projection, with high-symmetry points indicated. With decreasing temperature from room temperature, the magnetic moment first follows a Curie-Weiss behavior, then shows a sudden reduction below 106 K (Figure 1c), indicating an AFM transition. In the AFM state, the magnetic moments of Cr atoms align in an A-type AFM form along the out-of-plane direction with intralayer FM order (Figure 1a). Figure 1d shows the constant-energy contours around $\bar{\Gamma}$ at different binding energies. We observe two hole pockets α_1 and α_2 on the Fermi surface and another two hole pockets δ_1 and δ_2 in the constant-energy contours below about -0.1 eV.

Figures 2a and 2b show the measured band dispersions along the $\bar{\Gamma}\bar{K}$ and $\bar{\Gamma}\bar{M}$ directions, respectively. We observe two hole bands α_1 and α_2 crossing E_F with similar Fermi velocities. At higher binding energies, there exist two extra hole bands δ_1 and δ_2 (Figure 2a). To unravel the origin of the two sets of splitting-like energy bands, we perform *ab-initio* calculations of the band structure of bulk NaCrTe₂ in the AFM state. Nevertheless, the calculation clearly deviates from the measured band structure as compared in Figures 2a-2c. The calculation of NaCrTe₂ not only overestimates the Fermi momenta of the energy bands but also suggests a clear anisotropy of the band splitting along $\bar{\Gamma}\bar{K}$ and $\bar{\Gamma}\bar{M}$. Moreover, there are three hole bands between -0.2 and -0.6 eV in the calculation instead of two hole bands in the experiment.

It is interesting to note that the experimental results are similar to those of CrTe₂ films¹¹. Indeed, the calculation of monolayer CrTe₂ well reproduces the experimental results (Figure 2d). Figures 2e-2h compare the experimental and calculated band structures in a large energy and momentum range (Supporting Information, Figure S1). Again, the experiments fit much better to the calculation of monolayer CrTe₂ in the FM state than that of bulk NaCrTe₂ in the AFM state. Considering the surface sensitivity of ARPES experiments, we argue that the ARPES spectra of NaCrTe₂ are dominated by the photoelectrons emitted from the surface layer of Na-decorated CrTe₂.

To further decipher the nature of the observed splitting-like band dispersions, we perform detailed temperature-dependent ARPES measurements. As shown in Figure 3a, with increasing temperature, the α_1 and α_2 bands gradually approach each other and finally merge into one band α at 142 K. By fitting the momentum distribution curves (MDCs) at E_F (see Figure 3b and Supporting Information Figure S4 for details), we can track the temperature evolution of the band splitting. As shown in Figure 3c, the observed band splitting resembles the behavior of a typical FM exchange splitting. To quantify the FM transition temperature, we fit the band splitting by the Weiss mean-field model (see Supporting Information Figure S6 for the fit of the data to Landau's phase transition theory)³¹.

For the $J = 3/2$ system as in CrTe₂²⁶, the model gives

$$\frac{M(T)}{M_s} = B_J \left(\frac{3J}{J+1} \cdot \frac{M(T)}{M_s} \cdot \frac{T_c}{T} \right) = \frac{4}{3} \coth \left(\frac{12 M(T) T_c}{5 M_s T} \right) - \frac{1}{3} \coth \left(\frac{3 M(T) T_c}{5 M_s T} \right) \quad (1),$$

where M_s is the saturated magnetization, and $B_J(x)$ is the Brillouin function. Using this model, we obtain a critical temperature of $T_c = 128 \pm 4$ K (Figure 3c), well above the bulk $T_N = 106$ K. Similar

analysis applies for the energy distribution curves (EDCs) at $k_{\parallel} = 0.24 \text{ \AA}^{-1}$ (see Figure 2d and Supporting Information, Figure S5), which gives $T_c = 125 \pm 5 \text{ K}$ (Figure 3e). It is worth mentioning that the splitting of δ_1 and δ_2 bands shows exactly the same behavior (Supporting Information, Figure S3).

The comparison between ARPES experiments and *ab-initio* calculations, together with the temperature evolution of the band structure, compellingly evidences a surface FM state. Considering the A-type AFM property of NaCrTe_2 and the previously reported room-temperature ferromagnetism in ultrathin CrTe_2 films^{11,27}, we argue that the observed exchange splitting is due to the quantum-confined FM state on the topmost surface of the system. We should also note that the strong temperature dependence of the exchange splitting that fits to the mean-field model is indicative of an itinerant FM state on the sample surface³²⁻³⁴.

Interestingly, the surface ferromagnetism can be feasibly controlled by surface doping of alkali-metal atoms. As shown in Figures 4a-4d, the band splitting sensitively responds to the surface doping of Rb atoms. With increasing doping level, the α_1 and α_2 bands shift towards higher binding energies and the exchange splitting reduces. After surface doping for about 335 s, the α_1 and α_2 bands submerge below E_F , indicating a surface-doping-induced Lifshitz transition. Finally, the exchange splitting vanishes as summarized in Figure 4e. It is noteworthy that the chemical potential can be effectively tuned for more than 500 meV, suggesting an efficient tunability. More importantly, after the topmost CrTe_2 layer is covered by the doped alkali-metal atoms, the band structure

becomes in good agreement with the *ab-initio* calculation of non-magnetic NaCrTe₂ (Supporting Information, Figure S2), confirming the suppression of the surface ferromagnetism.

We emphasize that the T_c of the surface ferromagnetism is also tunable by surface doping. As shown in Figure 4f, we first dope Rb atoms on the sample surface for 120 s to partially suppress the exchange splitting, then conduct temperature-dependent measurements to determine the T_c at this doping level. The subsequent temperature-dependent measurements (Figures 4g-4i) show a similar temperature evolution of the exchange splitting as in Figure 3. But the splitting now disappears at about 108 K (Figure 4j), well below that in the sample without doping, suggesting the T_c of the surface ferromagnetism is lowered. In principle, the tunability of the ferromagnetism can be established either by modifying the exchange interaction between magnetic moments mediated by carrier density or by changing the electronic band structure, particularly the density of states (DOS) near E_F , as represented by the Ruderman–Kittel–Kasuya–Yosida (RKKY) and Stoner mechanism, respectively.

In vdW magnets, the interlayer magnetic coupling is usually one or two orders of magnitude weaker than the intralayer coupling. This leaves the possibility for the intermediate states where the interlayer magnetic order is quenched while the intralayer magnetic order survives during magnetic transitions^{26,27}. However, it is unexpected to observe such a large FM exchange splitting on the surface of AFM materials by ARPES^{16,35-37}. Similar band splitting with much smaller energy scale was also observed on the surface of antiferromagnetic topological insulator MnBi₂Te₄, whose origin

awaits further investigation^{36, 38, 39}. In the 3D AFM rare-earth heavy fermion compound EuRh_2Si_2 ¹⁶, surface electrons are polarized by the magnetic proximity effect, forming itinerant surface ferromagnetism; In transition metal oxide PbCoO_2 , the enhanced surface density of states drives the Stoner transition⁴⁰. However, both of them depend on the surface termination with relatively low T_c . On the contrary, the observed ferromagnetism is inherited from the 2D magnetism of monolayer CrTe_2 . Therefore, the T_c of the quantum-confined surface ferromagnetism here is much higher. By doping or removing alkali-metal atoms on the sample surface, the T_c of the surface FM state can in principle be tuned in a large temperature range, which provides an ideal and unique playground for further exploration. On the other hand, the asymmetric coverage of alkali-metal atoms on the top and bottom of the surface CrTe_2 layer alludes to a large Dzyaloshinskii-Moriya interaction (DMI)⁴¹, which is beneficial for the non-centrosymmetric FM order^{42, 43}, which may play an important role in the observed surface FM state.

In summary, we observe an unusual exchange splitting on the surface of a vdW AFM material, Na-intercalated CrTe_2 , by ARPES and *ab-initio* calculation. The T_c of the quantum-confined 2D FM state is well above the bulk AFM T_N . Both the magnitude of the exchange splitting and the T_c of the surface ferromagnetism can be effectively tuned by the surface doping of alkali-metal atoms. Our work provides not only a rare platform to explore the intra- and inter-layer magnetic interactions in vdW materials but also a feasible method to tune their magnetic properties.

Methods

High-quality NaCrTe₂ single crystals were synthesized using the self-flux method²⁷. Synchrotron-based ARPES experiments were performed at beamline ULTRA at the Swiss Light Source (SLS) using a Scienta DA30L analyzer. The convolved energy and angular resolutions were set to 15 meV and 0.2°, respectively. Laser-based ARPES experiments were performed at Tsinghua University using a Scienta DA30 analyzer and a 7 eV laser source. The overall energy and angular resolutions were 3 meV and 0.2°, respectively. The samples were cleaved *in-situ* and measured under ultrahigh vacuum below 6×10^{-11} mbar. First-principles band structure calculations were performed using QUANTUM ESPRESSO code package⁴⁴ with a plane-wave basis. The exchange-correlation energy was considered under Perdew-Burke-Ernzerhof (PBE) type generalized gradient approximation (GGA)⁴⁵ with spin-orbit coupling included. Hubbard $U = 4.0$ eV was applied to describe the localized 3*d* orbitals of Cr atoms^{46,47}. The cut-off energy for the plane-wave basis was set to 600 eV. A Γ -centered Monkhorst-Pack *k*-point mesh of 13×13×3 was adopted in the self-consistent calculations.

ASSOCIATED CONTENT

Data Availability Statement

The data sets that support the findings of this study are available from the corresponding author upon reasonable request.

Supporting Information

The Supporting Information is available free of charge at [URL to be inserted].

Photon energy-dependent measurements of NaCrTe₂, comparison between the experimental and calculated band structure of non-magnetic CrTe₂ and NaCrTe₂, temperature-dependent energy splitting of the δ_1 and δ_2 bands extracted from the energy distribution curves at the $\bar{\Gamma}$ point, fitting details of the temperature-dependent momentum distribution curves, fitting details of the temperature-dependent energy distribution curves, fit of the temperature evolution of the band splitting to Landau's phase transition theory, and second derivative and curvature analysis of the band dispersions.

Author Contributions

L.X.Y. conceived the scientific project. Y.D.L., J.Y.L., H.K.C., Y.H.Y. carried out ARPES measurements and data analyses with the assistance of X.D., R.Z.X., W.X.Z., K.Y.Z., N.C.P., S.L.J., M.S., Z.K.L., and Y.L.C. X.D. performed the *ab-initio* calculations. Single crystals were synthesized and characterized by J.J.W., J.G.G. and X.L.C. All authors contributed to the scientific planning and discussion.

Notes

Authors declare that they have no competing interests.

ACKNOWLEDGMENTS

This work is funded by the National Key R&D Program of China (No. 2022YFA1403100 and No. 2022YFA1403200), the Beijing Natural Science Foundation (Grant No. Z200005), the National Natural Science Foundation of China (Grants No. 12275148). L. X. Y. acknowledges the support from Tsinghua University Initiative Scientific Research Program. The experiments in PSI are conducted under the proposal ID: 20211981.

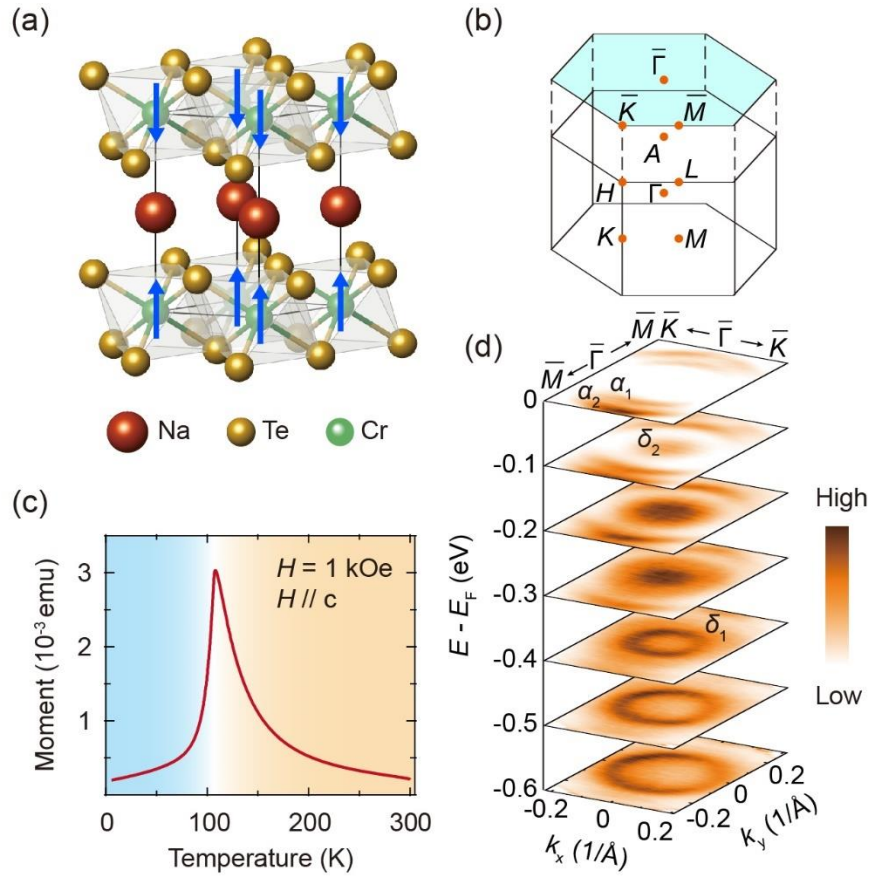


Figure 1. Basic Properties of NaCrTe₂. (a) Schematic of the crystal structure of NaCrTe₂. The blue arrows indicate the magnetic moment orientations of Cr atoms in the A-type antiferromagnetic (AFM) state. (b) Three-dimensional (3D) Brillouin zone (BZ) of NaCrTe₂ and its surface projection with high symmetry points indicated. (c) Field-cooled magnetization as a function of temperature showing the AFM transition at 106 K. (d) Constant-energy contours around $\bar{\Gamma}$ at selected binding energies.

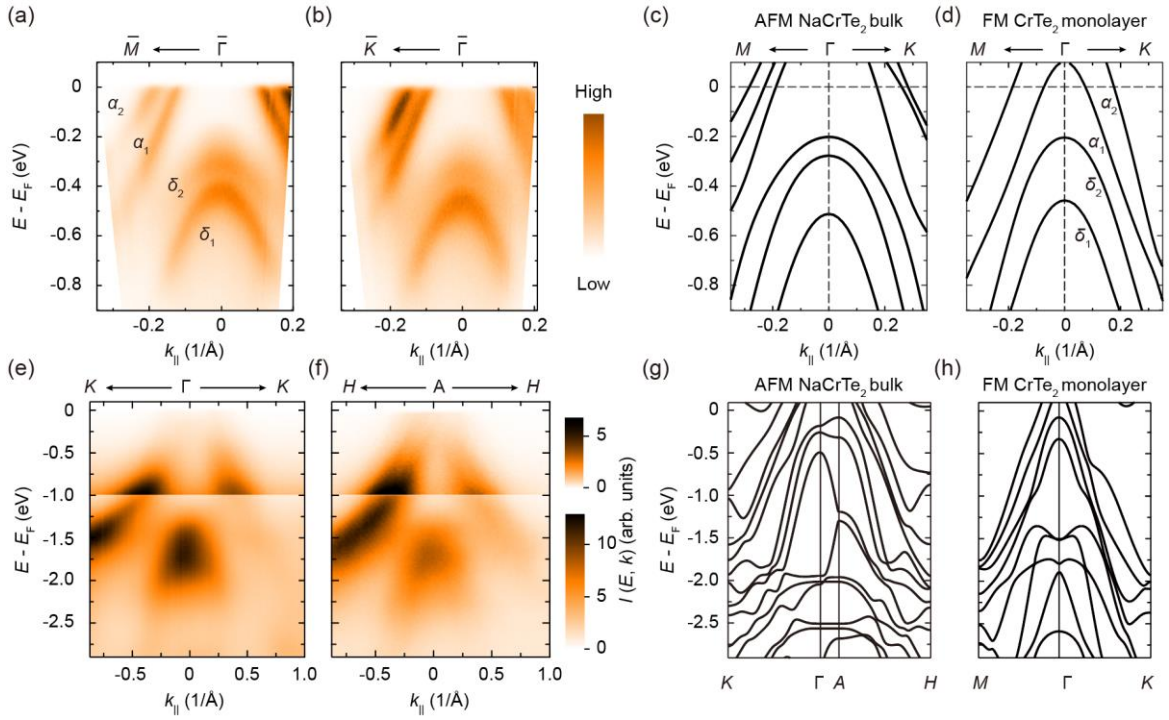


Figure 2. Comparisons between experimental and calculated band structures. (a,b) Band dispersions of NaCrTe₂ along the $\bar{\Gamma}\bar{M}$ (a) and $\bar{\Gamma}\bar{K}$ (b) directions. Data were collected using linearly (LH) polarized 7 eV laser at 80 K. (c) Calculated band structure of bulk NaCrTe₂ in the AFM state. (d) Calculated band structure of monolayer CrTe₂ in the ferromagnetic (FM) state. (e,f) Band dispersions of bulk NaCrTe₂ along the AH and ΓK directions. Data were collected using 75 eV and 100 eV photons with LH polarization at 20 K. The contrast of ARPES spectra above -1.0 eV was separately adjusted to enhance the states near the Fermi level (E_F). (g,h) Calculated band structures of bulk NaCrTe₂ in the AFM state (g) and monolayer CrTe₂ in the FM state (h).

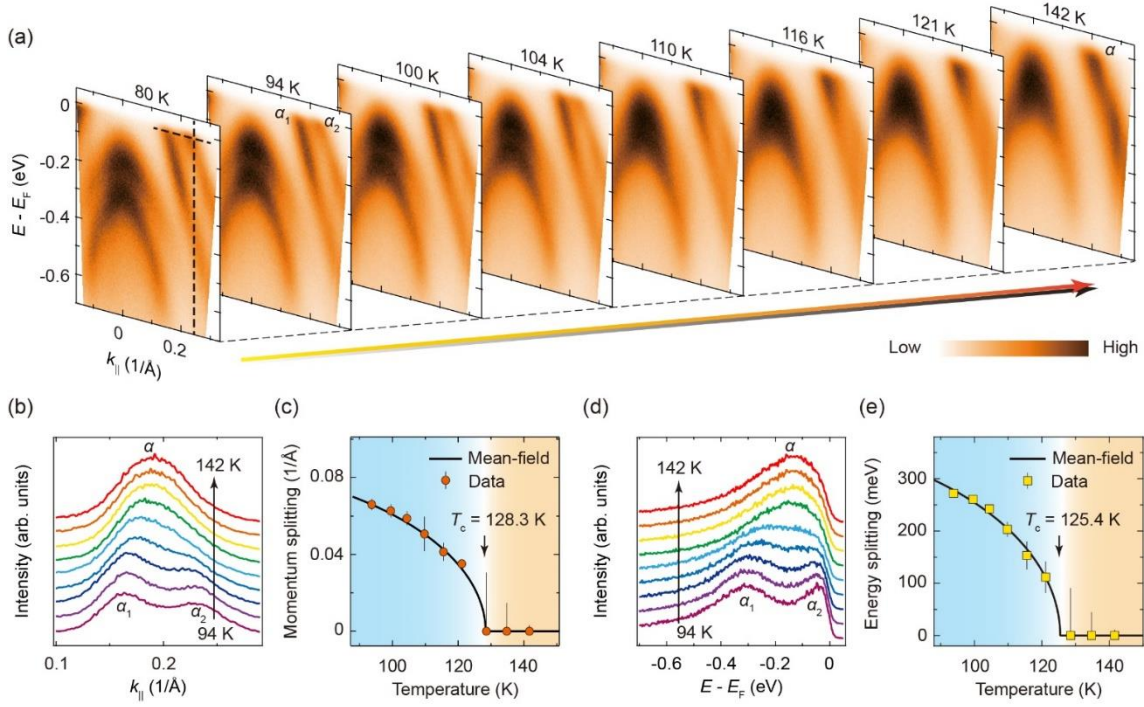


Figure 3. Temperature dependence of the unusual exchange splitting. (a) Temperature evolution of the band dispersion along the $\bar{\Gamma}\bar{M}$ direction. (b) Momentum distribution curves (MDCs) at selected temperatures showing the evolution of the exchange splitting. (c) Momentum splitting at E_F [horizontal dashed line in the panel (a)] as a function of temperature. The black line is the fit of the data to the mean-field model. (d) Energy distribution curves (EDCs) at selected temperatures showing the evolution of the exchange splitting. (e) Energy splitting along the vertical dashed line in the panel (a) as a function of temperature. The black line is the fit of the data to the mean-field model.

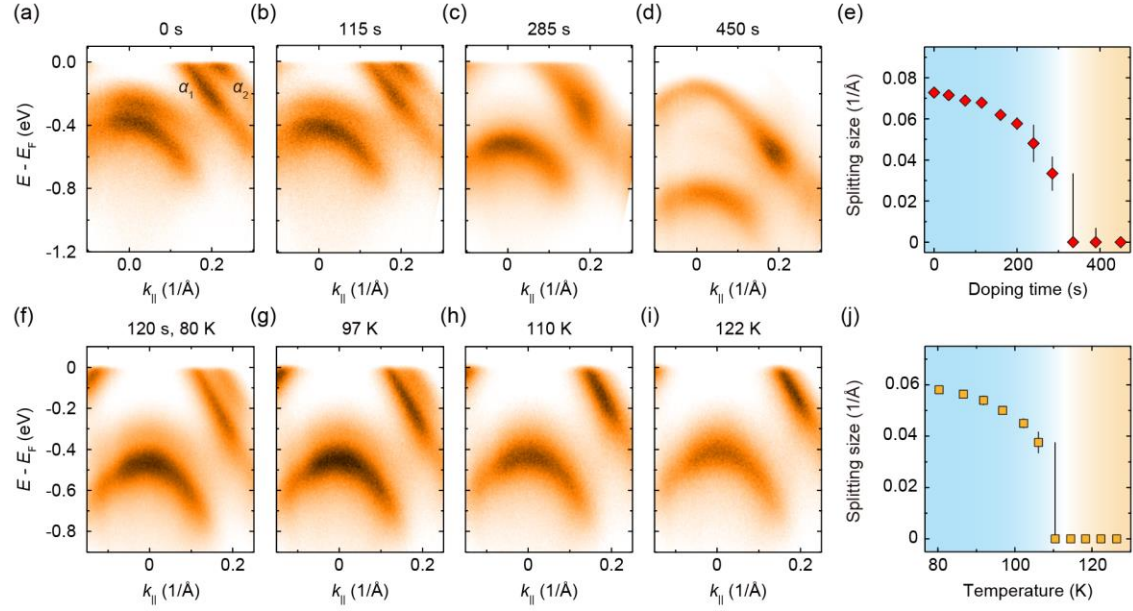


Figure 4. Tunability of the surface ferromagnetism in NaCrTe₂ by alkali-metal atoms doping.

(a-d) Evolution of the band dispersion with surface doping time. The exchange splitting reduces and finally disappears at high doping levels. (e) Summary of the momentum splitting of the α_1 and α_2 bands at E_F as a function of surface doping time. (f) Band structure of NaCrTe₂ with slight surface doping of Rb atoms. The exchange splitting is partially suppressed. (g-i) Band dispersions of the slightly doped NaCrTe₂ at selected temperatures. (j) Momentum splitting of the α_1 and α_2 bands in the slightly doped sample as a function of temperature.

REFERENCES

1. Mermin, N. D.; Wagner, H. Absence of Ferromagnetism or Antiferromagnetism in One- or Two-Dimensional Isotropic Heisenberg Models. *Phys. Rev. Lett.* **1966**, 17, (22), 1133-1136.
2. Gibertini, M.; Koperski, M.; Morpurgo, A. F.; Novoselov, K. S. Magnetic 2D materials and

heterostructures. *Nat. Nanotechnol.* **2019**, 14, (5), 408-419.

3. Mak, K. F.; Shan, J.; Ralph, D. C. Probing and controlling magnetic states in 2D layered magnetic materials. *Nat. Rev. Phys.* **2019**, 1, (11), 646-661.

4. Gong, C.; Zhang, X. Two-dimensional magnetic crystals and emergent heterostructure devices. *Science* **2019**, 363, (6428), 706.

5. Huang, B.; McGuire, M. A.; May, A. F.; Xiao, D.; Jarillo-Herrero, P.; Xu, X. D. Emergent phenomena and proximity effects in two-dimensional magnets and heterostructures. *Nat. Mater.* **2020**, 19, (12), 1276-1289.

6. Burch, K. S.; Mandrus, D.; Park, J. G. Magnetism in two-dimensional van der Waals materials. *Nature* **2018**, 563, (7729), 47-52.

7. Gong, C.; Li, L.; Li, Z.; Ji, H.; Stern, A.; Xia, Y.; Cao, T.; Bao, W.; Wang, C.; Wang, Y.; Qiu, Z. Q.; Cava, R. J.; Louie, S. G.; Xia, J.; Zhang, X. Discovery of intrinsic ferromagnetism in two-dimensional van der Waals crystals. *Nature* **2017**, 546, (7657), 265-269.

8. Huang, B.; Clark, G.; Navarro-Moratalla, E.; Klein, D. R.; Cheng, R.; Seyler, K. L.; Zhong, D.; Schmidgall, E.; McGuire, M. A.; Cobden, D. H.; Yao, W.; Xiao, D.; Jarillo-Herrero, P.; Xu, X. D. Layer-dependent ferromagnetism in a van der Waals crystal down to the monolayer limit. *Nature* **2017**, 546, (7657), 270-273.

9. Bonilla, M.; Kolekar, S.; Ma, Y.; Diaz, H. C.; Kalappattil, V.; Das, R.; Eggers, T.; Gutierrez, H. R.; Phan, M.-H.; Batzill, M. Strong room-temperature ferromagnetism in VSe₂ monolayers on van der Waals substrates. *Nat. Nanotechnol.* **2018**, 13, (4), 289-293.

10. O'Hara, D. J.; Zhu, T.; Trout, A. H.; Ahmed, A. S.; Luo, Y. K.; Lee, C. H.; Brenner, M. R.; Rajan, S.; Gupta, J. A.; McComb, D. W.; Kawakami, R. K. Room Temperature Intrinsic Ferromagnetism in Epitaxial Manganese Selenide Films in the Monolayer Limit. *Nano Lett.* **2018**, 18, (5), 3125-3131.
11. Zhang, X. Q.; Lu, Q. S.; Liu, W. Q.; Niu, W.; Sun, J. B.; Cook, J.; Vaninger, M.; Miceli, P. F.; Singh, D. J.; Lian, S. W.; Chang, T. R.; He, X. Q.; Du, J.; He, L.; Zhang, R.; Bian, G.; Xu, Y. B. Room-temperature intrinsic ferromagnetism in epitaxial CrTe₂ ultrathin films. *Nat. Commun.* **2021**, 12, (1), 2492.
12. Deng, Y. J.; Yu, Y. J.; Shi, M. Z.; Guo, Z. X.; Xu, Z. H.; Wang, J.; Chen, X. H.; Zhang, Y. B. Quantum anomalous Hall effect in intrinsic magnetic topological insulator MnBi₂Te₄. *Science* **2020**, 367, (6480), 895-900.
13. Mogi, M.; Kawamura, M.; Yoshimi, R.; Tsukazaki, A.; Kozuka, Y.; Shirakawa, N.; Takahashi, K. S.; Kawasaki, M.; Tokura, Y. A magnetic heterostructure of topological insulators as a candidate for an axion insulator. *Nat. Mater.* **2017**, 16, (5), 516-521.
14. Herrera, E.; Guillamón, I.; Barrena, V.; Herrera, W. J.; Galvis, J. A.; Yeyati, A. L.; Rusz, J.; Oppeneer, P. M.; Knebel, G.; Brison, J. P.; Flouquet, J.; Aoki, D.; Suderow, H. Quantum-well states at the surface of a heavy-fermion superconductor. *Nature* **2023**, 616, (7957), 465-469.
15. Bahramy, M. S.; King, P. D. C.; de la Torre, A.; Chang, J.; Shi, M.; Patthey, L.; Balakrishnan, G.; Hofmann, P.; Arita, R.; Nagaosa, N.; Baumberger, F. Emergent quantum confinement at topological insulator surfaces. *Nat. Commun.* **2012**, 3, (1), 1159.

16. Chikina, A.; Höppner, M.; Seiro, S.; Kummer, K.; Danzenbächer, S.; Patil, S.; Generalov, A.; Güttler, M.; Kucherenko, Y.; Chulkov, E. V.; Koroteev, Y. M.; Koepernik, K.; Geibel, C.; Shi, M.; Radovic, M.; Laubschat, C.; Vyalikh, D. V. Strong ferromagnetism at the surface of an antiferromagnet caused by buried magnetic moments. *Nat. Commun.* **2014**, *5*, (1), 3171.
17. Wang, H.; Wen, Y.; Zhao, X.; Cheng, R.; Yin, L.; Zhai, B.; Jiang, J.; Li, Z.; Liu, C.; Wu, F.; He, J. Heteroepitaxy of 2D CuCr_2Te_4 with Robust Room-temperature Ferromagnetism. *Adv. Mater.* **2023**, *35*, (18), e2211388.
18. Wen, Y.; Liu, Z.; Zhang, Y.; Xia, C.; Zhai, B.; Zhang, X.; Zhai, G.; Shen, C.; He, P.; Cheng, R.; Yin, L.; Yao, Y.; Getaye Sendeku, M.; Wang, Z.; Ye, X.; Liu, C.; Jiang, C.; Shan, C.; Long, Y.; He, J. Tunable Room-Temperature Ferromagnetism in Two-Dimensional Cr_2Te_3 . *Nano Lett.* **2020**, *20*, (5), 3130-3139.
19. Sun, X. D.; Li, W. Y.; Wang, X.; Sui, Q.; Zhang, T. Y.; Wang, Z.; Liu, L.; Li, D.; Feng, S.; Zhong, S. Y.; Wang, H. W.; Bouchiat, V.; Regueiro, M. N.; Rougemaille, N.; Coraux, J.; Purbawati, A.; Hadj-Azzem, A.; Wang, Z. H.; Dong, B. J.; Wu, X.; Yang, T.; Yu, G. Q.; Wang, B. W.; Han, Z.; Han, X. F.; Zhang, Z. D. Room temperature ferromagnetism in ultra-thin van der Waals crystals of $1T\text{-CrTe}_2$. *Nano Res.* **2020**, *13*, (12), 3358-3363.
20. Huang, M.; Ma, Z. W.; Wang, S.; Li, S.; Li, M.; Xiang, J. X.; Liu, P.; Hu, G. J.; Zhang, Z. M.; Sun, Z.; Lu, Y. L.; Sheng, Z. G.; Chen, G.; Chueh, Y. L.; Yang, S. Y.; Xiang, B. Significant perpendicular magnetic anisotropy in room-temperature layered ferromagnet of Cr-intercalated CrTe_2 . *2D Mater.* **2021**, *8*, (3), 031003.

21. Meng, L. J.; Zhou, Z.; Xu, M. Q.; Yang, S. Q.; Si, K. P.; Liu, L. X.; Wang, X. G.; Jiang, H. N.; Li, B. X.; Qin, P. X.; Zhang, P.; Wang, J. L.; Liu, Z. Q.; Tang, P. Z.; Ye, Y.; Zhou, W.; Bao, L. H.; Gao, H. J.; Gong, Y. J. Anomalous thickness dependence of Curie temperature in air-stable two-dimensional ferromagnetic $1T\text{-CrTe}_2$ grown by chemical vapor deposition. *Nat. Commun.* **2021**, *12*, (1), 809.
22. Huang, M.; Wang, S.; Wang, Z.; Liu, P.; Xiang, J.; Feng, C.; Wang, X.; Zhang, Z.; Wen, Z.; Xu, H.; Yu, G.; Lu, Y.; Zhao, W.; Yang, S. A.; Hou, D.; Xiang, B. Colossal Anomalous Hall Effect in Ferromagnetic van der Waals CrTe_2 . *ACS Nano* **2021**, *15*, (6), 9759-9763.
23. Zheng, H.; Huang, C.; Lin, F. R.; Fan, J. Y.; Liu, H.; Zhang, L.; Ma, C. L.; Wang, C. X.; Zhu, Y.; Yang, H. Two-dimensional van der Waals ferromagnetic thin film CrTe_2 with high Curie temperature and metallic conductivity. *Appl. Phys. Lett.* **2023**, *122*, (2), 023103.
24. Xian, J. J.; Wang, C.; Nie, J. H.; Li, R.; Han, M. J.; Lin, J. H.; Zhang, W. H.; Liu, Z. Y.; Zhang, Z. M.; Miao, M. P.; Yi, Y. F.; Wu, S. W.; Chen, X. D.; Han, J. B.; Xia, Z. C.; Ji, W.; Fu, Y. S. Spin mapping of intralayer antiferromagnetism and field-induced spin reorientation in monolayer CrTe_2 . *Nat. Commun.* **2022**, *13*, (1), 257.
25. Freitas, D. C.; Weht, R.; Sulpice, A.; Remenyi, G.; Strobel, P.; Gay, F.; Marcus, J.; Núñez-Regueiro, M. Ferromagnetism in layered metastable $1T\text{-CrTe}_2$. *J. Phys. Condens. Matter* **2015**, *27*, (17), 176002.
26. Huang, J.; Shi, B.; Pan, F.; Wang, J.; Liu, J.; Xu, D.; Zhang, H.; Xia, T.; Cheng, P. Anisotropic magnetic properties and tunable conductivity in two-dimensional layered NaCrX_2 ($X=\text{Te,Se,S}$)

single crystals. *Phys. Rev. Mater.* **2022**, 6, (9), 094013.

27. Wang, J. J.; Deng, J.; Liang, X. W.; Gao, G. Y.; Ying, T. P.; Tian, S. J.; Lei, H. C.; Song, Y. P.; Chen, X.; Guo, J. G.; Chen, X. L. Spin-flip-driven giant magnetotransport in A-type antiferromagnet NaCrTe₂. *Phys. Rev. Mater.* **2021**, 5, (9), L091401.

28. Xu, W.; Ali, S.; Jin, Y.; Wu, X.; Xu, H. Intrinsic Ferromagnetic Semiconductors in Two-Dimensional Alkali-Based Chromium Chalcogenides. *ACS Applied Electronic Materials* **2020**, 2, (12), 3853-3858.

29. Gao, P.; Li, X.; Yang, J. Thickness Dependent Magnetic Transition in Few Layer 1T Phase CrTe₂. *J. Phys. Chem. Lett.* **2021**, 12, (29), 6847-6851.

30. Wu, L. L.; Zhou, L. W.; Zhou, X. Y.; Wang, C.; Ji, W. In-plane epitaxy-strain-tuning intralayer and interlayer magnetic coupling in CrSe₂ and CrTe₂ monolayers and bilayers. *Phys. Rev. B* **2022**, 106, (8), L081401.

31. Getzlaff, M., *Fundamentals of Magnetism*. Springer: New York, 2008.

32. Qin, N.; Chen, C.; Du, S. Q.; Du, X.; Zhang, X.; Yin, Z. X.; Zhou, J. S.; Xu, R. Z.; Gu, X.; Zhang, Q. Q.; Zhao, W. X.; Li, Y. D.; Mo, S. K.; Liu, Z. K.; Zhang, S. L.; Guo, Y. F.; Tang, P. Z.; Chen, Y. L.; Yang, L. X. Persistent exchange splitting in the chiral helimagnet Cr_{1/3}NbS₂. *Phys. Rev. B* **2022**, 106, (3), 035129.

33. Xu, X.; Li, Y. W.; Duan, S. R.; Zhang, S. L.; Chen, Y. J.; Kang, L.; Liang, A. J.; Chen, C.; Xia, W.; Xu, Y.; Malinowski, P.; Xu, X. D.; Chu, J. H.; Li, G.; Guo, Y. F.; Liu, Z. K.; Yang, L. X.; Chen, Y. L. Signature for non-Stoner ferromagnetism in the van der Waals ferromagnet Fe₃GeTe₂. *Phys.*

Rev. B **2020**, 101, (20), 201104.

34. Eastman, D. E.; Himpsel, F. J.; Knapp, J. A. Experimental Band-Structure and Temperature-Dependent Magnetic Exchange Splitting of Nickel Using Angle-Resolved Photoemission. *Phys. Rev. Lett.* **1978**, 40, (23), 1514-1517.

35. Yang, L. X.; Zhang, Y.; Ou, H. W.; Zhao, J. F.; Shen, D. W.; Zhou, B.; Wei, J.; Chen, F.; Xu, M.; He, C.; Chen, Y.; Wang, Z. D.; Wang, X. F.; Wu, T.; Wu, G.; Chen, X. H.; Arita, M.; Shimada, K.; Taniguchi, M.; Lu, Z. Y.; Xiang, T.; Feng, D. L. Electronic Structure and Unusual Exchange Splitting in the Spin-Density-Wave State of the BaFe₂As₂ Parent Compound of Iron-Based Superconductors. *Phys. Rev. Lett.* **2009**, 102, (10), 107002.

36. Chen, Y. J.; Xu, L. X.; Li, J. H.; Li, Y. W.; Wang, H. Y.; Zhang, C. F.; Li, H.; Wu, Y.; Liang, A. J.; Chen, C.; Jung, S. W.; Cacho, C.; Mao, Y. H.; Liu, S.; Wang, M. X.; Guo, Y. F.; Xu, Y.; Liu, Z. K.; Yang, L. X.; Chen, Y. L. Topological Electronic Structure and Its Temperature Evolution in Antiferromagnetic Topological Insulator MnBi₂Te₄. *Phys. Rev. X* **2019**, 9, (4), 041040.

37. Güttler, M.; Generalov, A.; Otrokov, M. M.; Kummer, K.; Kliemt, K.; Fedorov, A.; Chikina, A.; Danzenbächer, S.; Schulz, S.; Chulkov, E. V.; Koroteev, Y. M.; Caroca-Canales, N.; Shi, M.; Radovic, M.; Geibel, C.; Laubschat, C.; Dudin, P.; Kim, T. K.; Hoesch, M.; Krellner, C.; Vyalikh, D. V. Robust and tunable itinerant ferromagnetism at the silicon surface of the antiferromagnet GdRh₂Si₂. *Sci. Rep.* **2016**, 6, 24254.

38. Yang, S.; Xu, X.; Zhu, Y.; Niu, R.; Xu, C.; Peng, Y.; Cheng, X.; Jia, X.; Huang, Y.; Xu, X.; Lu, J.; Ye, Y. Odd-Even Layer-Number Effect and Layer-Dependent Magnetic Phase Diagrams in

MnBi₂Te₄. *Phys. Rev. X* **2021**, 11, (1), 011003.

39. Nguyen, K. D.; Lee, W.; Dang, J.; Wu, T.; Berruto, G.; Yan, C.; Ip, C. I. J.; Lin, H.; Gao, Q.; Lee, S. H.; Yan, B.; Liu, C.; Mao, Z.; Zhang, X.; Yang, S. Distinguishing Surface and Bulk Electromagnetism via Their Dynamics in an Intrinsic Magnetic Topological Insulator. *arXiv* **2024**, 2407.00281.

40. Mazzola, F.; Sunko, V.; Khim, S.; Rosner, H.; Kushwaha, P.; Clark, O. J.; Bawden, L.; Marković, I.; Kim, T. K.; Hoesch, M.; Mackenzie, A. P.; King, P. D. C. Itinerant ferromagnetism of the Pd-terminated polar surface of PdCoO₂. *Proc. Natl. Acad. Sci.* **2018**, 115, (51), 12956-12960.

41. Li, P.; Cui, Q. R.; Ga, Y. L.; Liang, J. H.; Yang, H. X. Large Dzyaloshinskii-Moriya interaction and field-free topological chiral spin states in two-dimensional alkali-based chromium chalcogenides. *Phys. Rev. B* **2022**, 106, (2), 024419.

42. Liu, Y.; Petrovic, C. Critical behavior of quasi-two-dimensional semiconducting ferromagnet Cr₂Ge₂Te₆. *Phys. Rev. B* **2017**, 96, (5), 054406.

43. Beutier, G.; Collins, S. P.; Dimitrova, O. V.; Dmitrienko, V. E.; Katsnelson, M. I.; Kvashnin, Y. O.; Lichtenstein, A. I.; Mazurenko, V. V.; Nisbet, A. G. A.; Ovchinnikova, E. N.; Pincini, D. Band Filling Control of the Dzyaloshinskii-Moriya Interaction in Weakly Ferromagnetic Insulators. *Phys. Rev. Lett.* **2017**, 119, (16), 167201.

44. Giannozzi, P.; Baroni, S.; Bonini, N.; Calandra, M.; Car, R.; Cavazzoni, C.; Ceresoli, D.; Chiarotti, G. L.; Cococcioni, M.; Dabo, I.; Dal Corso, A.; de Gironcoli, S.; Fabris, S.; Fratesi, G.; Gebauer, R.; Gerstmann, U.; Gougoussis, C.; Kokalj, A.; Lazzeri, M.; Martin-Samos, L.; Marzari,

- N.; Mauri, F.; Mazzarello, R.; Paolini, S.; Pasquarello, A.; Paulatto, L.; Sbraccia, C.; Scandolo, S.; Sclauzero, G.; Seitsonen, A. P.; Smogunov, A.; Umari, P.; Wentzcovitch, R. M. QUANTUM ESPRESSO: a modular and open-source software project for quantum simulations of materials. *J. Phys. Condens. Matter* **2009**, 21, (39), 395502.
45. Perdew, J. P.; Burke, K.; Ernzerhof, M. Generalized gradient approximation made simple. *Phys. Rev. Lett.* **1996**, 77, (18), 3865-3868.
46. Qin, N.; Du, X.; Lv, Y.; Kang, L.; Yin, Z.; Zhou, J.; Gu, X.; Zhang, Q.; Xu, R.; Zhao, W.; Li, Y.; Yao, S.; Chen, Y.; Liu, Z.; Yang, L.; Chen, Y. Electronic structure and spin-orbit coupling in ternary transition metal chalcogenides Cu_2TLX_2 ($X = \text{Se}, \text{Te}$). *Chin. Phys. B* **2022**, 31, (3), 037101
47. Shi, S.; Wysocki, A. L.; Belashchenko, K. D. Magnetism of chromia from first-principles calculations. *Phys. Rev. B* **2009**, 79, (10), 104404.